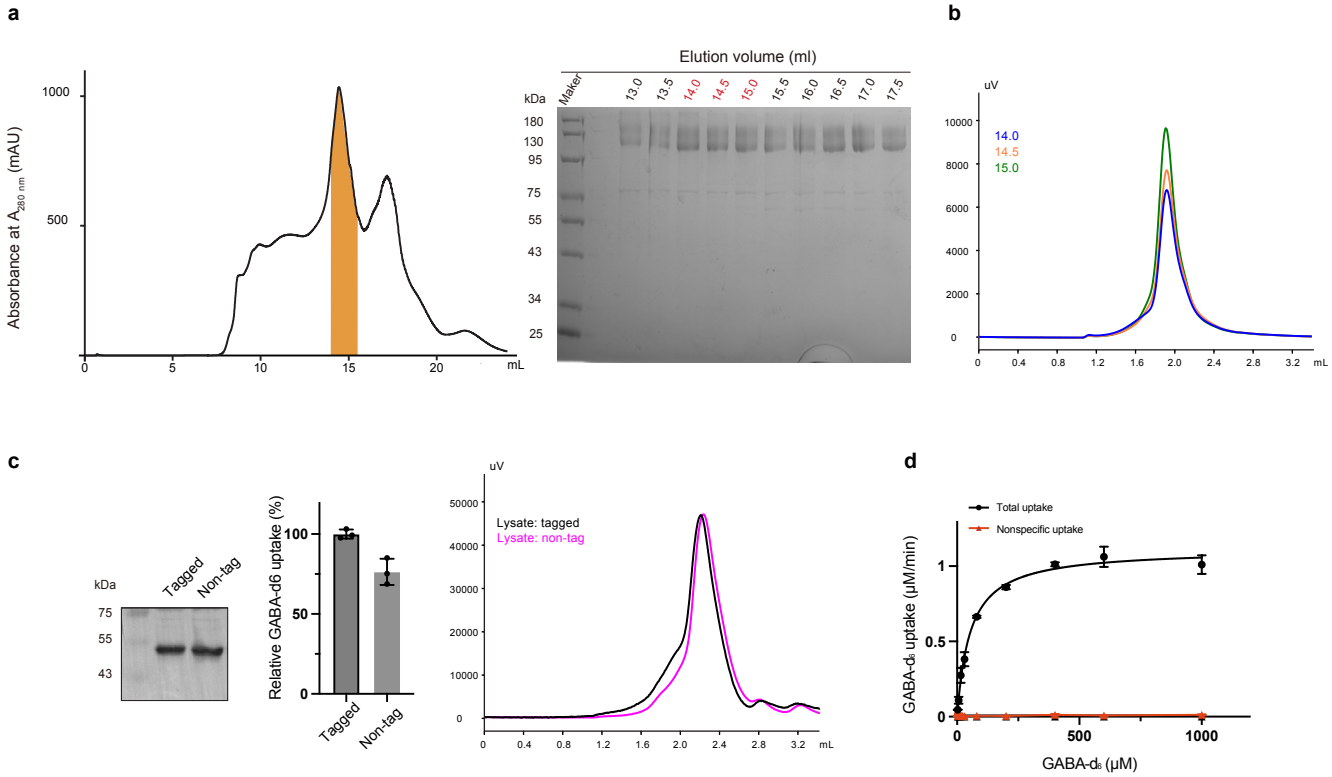

Supplementary Figure 1 | Purification and transport activity of hBGT1.
a. Size-exclusion chromatography (SEC) profile of purified hBGT1 in the presence of 0.025% (w/v) LMNG and 0.0025% (w/v) CHS. Absorbance at 280 nm was monitored. The yellow-shaded region (14.0–15.5 mL) indicates the fractions used for structural studies. Inset: SDS–PAGE analysis of peak fractions.
b. Fluorescence-detection size-exclusion chromatography (FSEC) profiles of SEC peak fractions at 14.0, 14.5, and 15.0 mL, used to assess the homogeneity and quality of hBGT1 protein.
c. Validation of the GFP–MBP-tagged hBGT1 construct. Western blot analysis, GABA-d_6 uptake activity, and size-exclusion chromatography profiles of tagged and non-tagged hBGT1 expressed in HEK293T cells indicate comparable expression and transport activity. Individual data points are shown; bars represent the mean ± s.d. (n = 3).
d. GABA-d_6 uptake activity of wild-type hBGT1. Both total and nonspecific uptake were measured; nonspecific uptake was determined in HEK293T cells infected with an empty vector, and only the specific uptake (total minus nonspecific) is presented in the main figures. Data were fitted to the Michaelis–Menten equation.Error bars represent the standard error of the mean (s.e.m.) from three independent experiments (n = 3).
Source data are provided as a Source Data file.

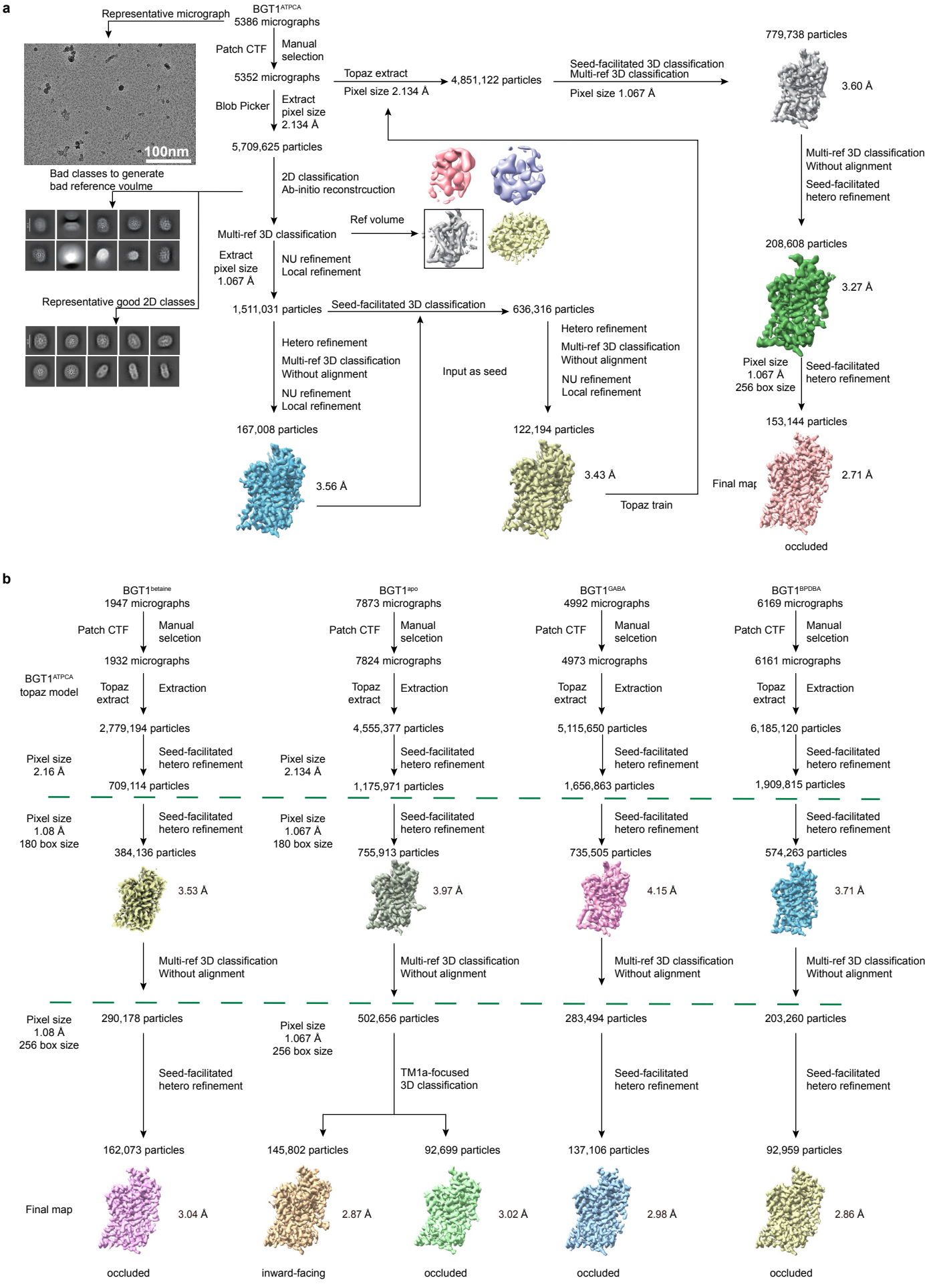

Supplementary Fig. 2 | Data processing of different hBGT1 datasets.
a. The flowchart for BGT1^{ATPCA} data processing. Detailed procedures are provided in the Methods section.
b. The flowchart for BGT1^{betaine}, BGT1^{apo}, BGT1^{GABA} and BGT1^{BPDBA} data processing. Detailed procedures are provided in the Methods section.

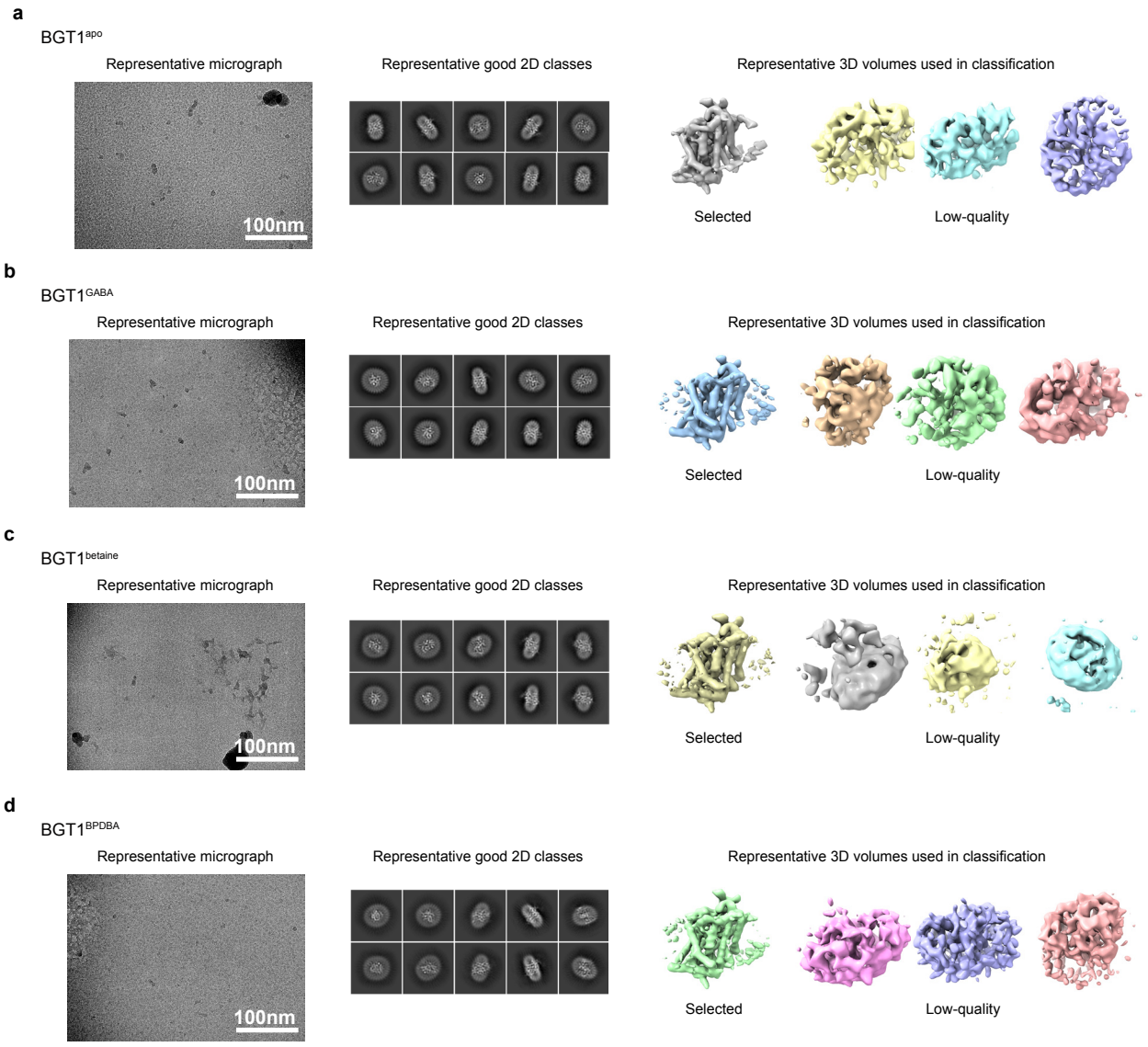

Supplementary Fig. 3 | Representative micrographs, 2D class averages, and 3D volumes used in classification of additional hBGT1 datasets.
a–d. Representative cryo-EM micrographs, selected good 2D class averages, and representative 3D volumes used in classification for the $BGT1^{apo}$ (a), $BGT1^{GABA}$ (b), $BGT1^{betaine}$ (c), and $BGT1^{BPDBA}$ (d) datasets. The selected 3D volume used for subsequent refinement is indicated in each panel.

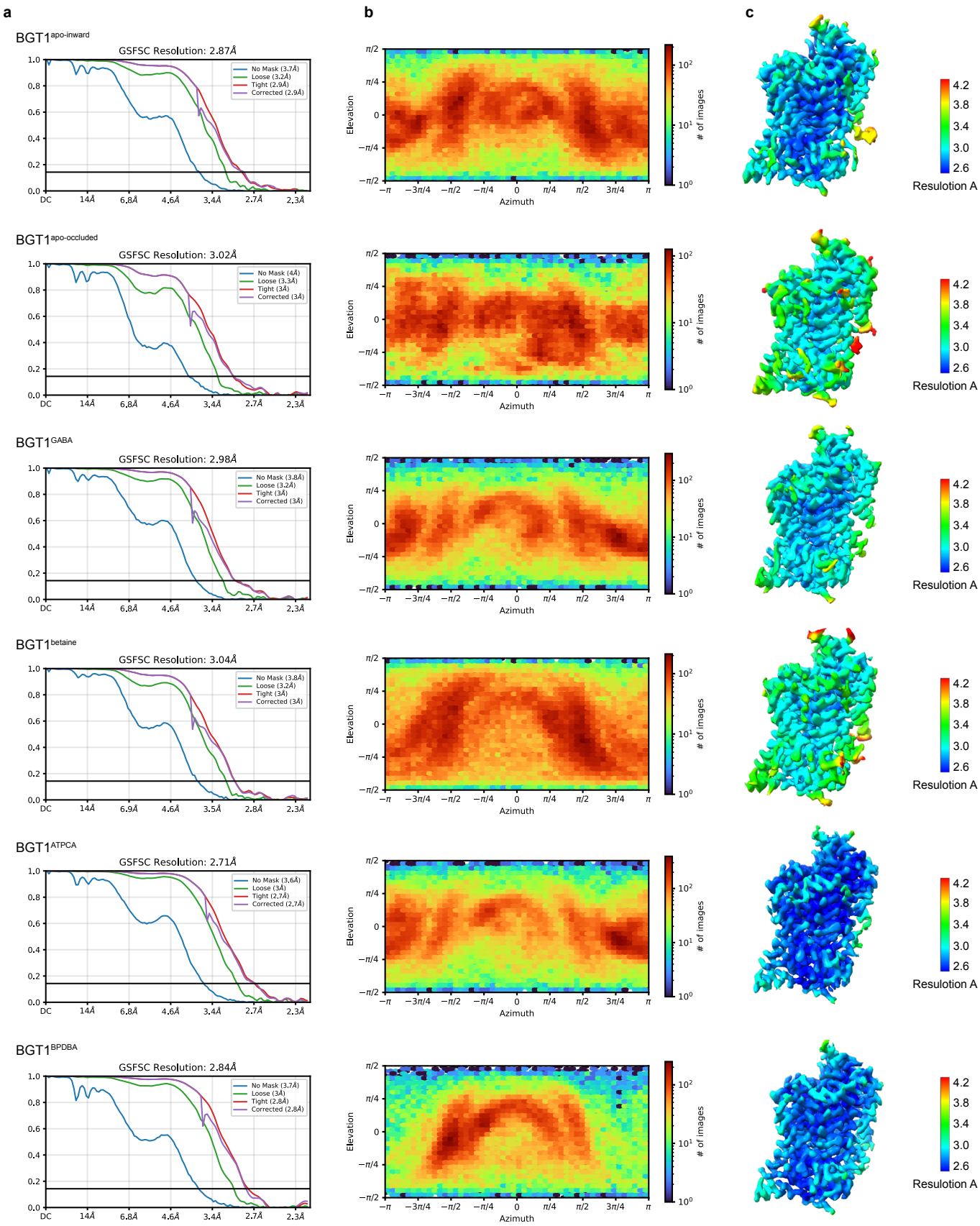

Supplementary Fig. 4 | Cryo-EM analysis of hBGT1 in different states.
a. Gold-standard Fourier shell correlation (FSC) curves for the overall 3D reconstructions of BGT1$^{apo\text{-}inward}$, BGT1$^{apo\text{-}occluded}$, BGT1^{GABA}, BGT1^{betaine}, BGT1^{ATPCA} and BGT1^{BPDBA}.
b. Angular distribution plots of particle orientations used for the final reconstructions.
c. Local resolution maps of the sharpened cryo-EM density maps, shown in front view for each structure at a contour level of 8σ.

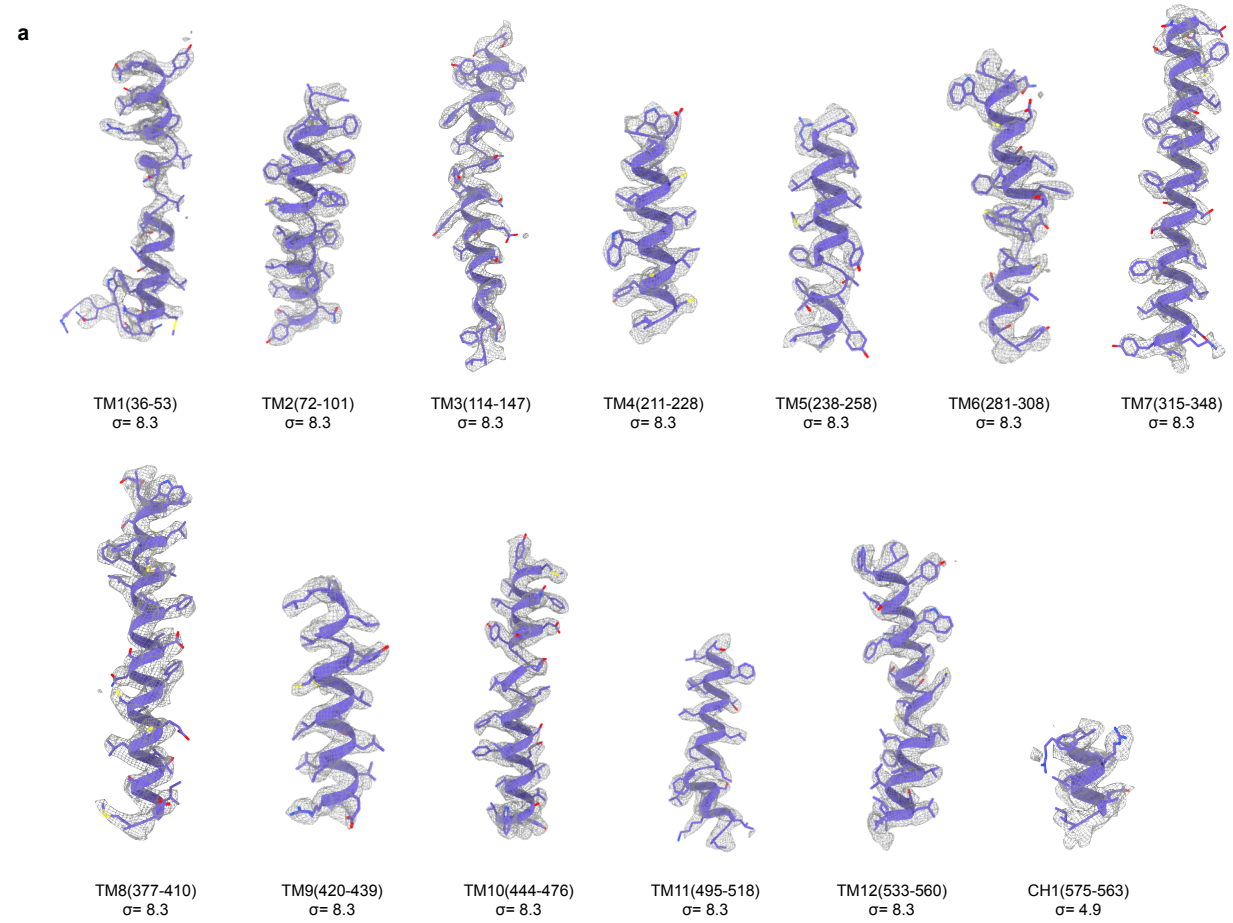

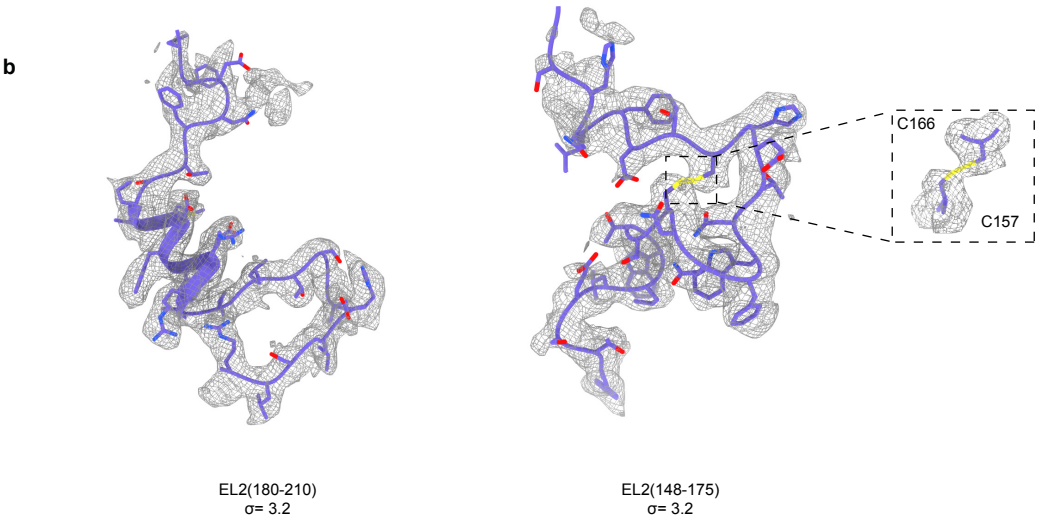

Supplementary Fig. 5 | Local density of hBGT1 in the occluded conformation.
a. Representative cryo-EM densities of transmembrane helices (TM) in the BPDBA-bound occluded-state structure. Maps are contoured at 8.3σ for TM helices and 4.9 σ for CH1.
b. Local density of the extracellular loop EL2, shown at a contour level of 3.2σ. Density clearly resolves the disulfide bond between C157 and C166. The disulfide bond is shown as yellow sticks.

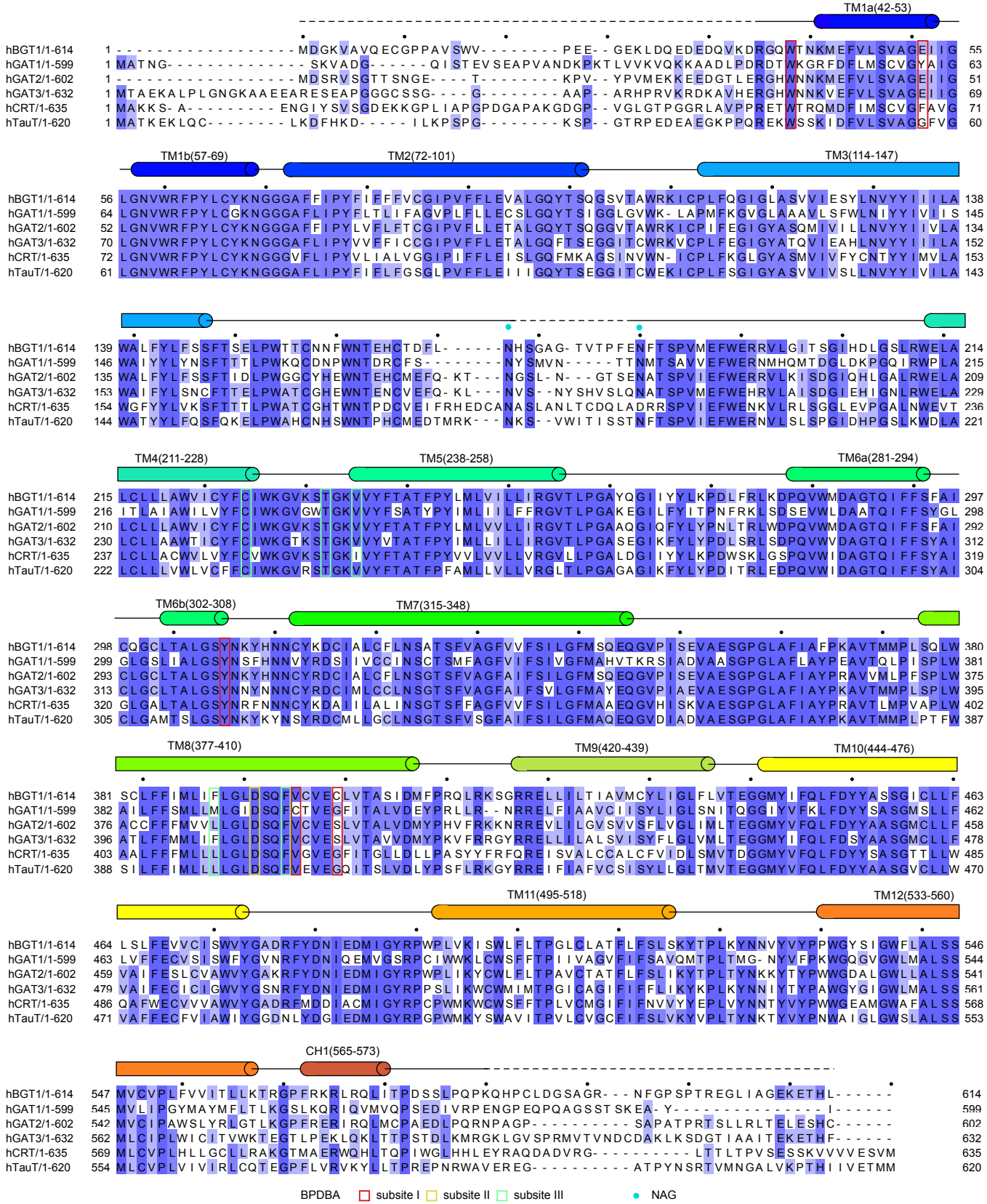

Supplementary Fig. 6 | Sequence alignment.
Multiple sequence alignment of hBGT1, hGAT1, hGAT2, hGAT3, hCRT1, and hTauT was performed using Jalview. Highly conserved residues are highlighted in purple. Transmembrane helices are represented as cylinders, with colors matching the rainbow scheme in Fig. 1a. Dotted lines indicate unmodeled regions. Glycosylation sites (N171 and N183) and residues involved in BPDBA binding are annotated.

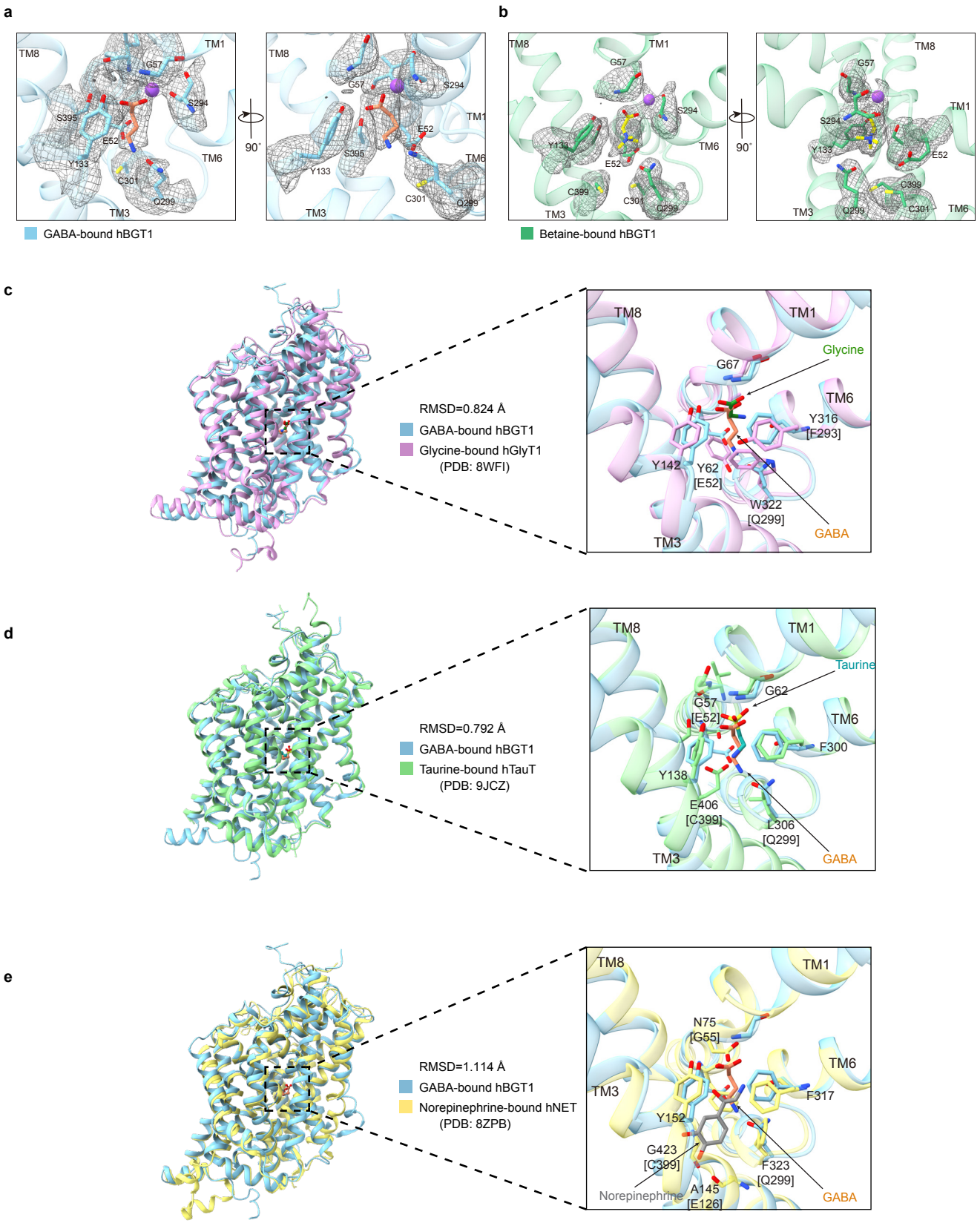

Supplementary Fig. 7 | Comparison of substrate-bound structures of hBGT1 with other SLC6A transporters.
a. Two orthogonal views of the substrate-binding pocket in GABA-bound hBGT1, with GABA and surrounding binding-site residues shown simultaneously in the cryo-EM density map (gray mesh), contoured at 5σ. Key interacting residues are labeled.
b. Two orthogonal views of the substrate-binding pocket in betaine-bound hBGT1, with betaine and surrounding binding-site residues shown simultaneously in the cryo-EM density map (gray mesh), contoured at 5σ. Key interacting residues are labeled.
c. Structural superposition of hBGT1 bound to GABA (this study, light blue) and hGlyT1 bound to glycine (PDB: 8WFI, pink). The substrate-binding pocket is enlarged (right) to show key residues Y62, G67, Y142, Y316, and W322.
d. Superposition of hBGT1–GABA (this study, light blue) and hTauT bound to taurine (PDB: 9JCZ, pale green). Binding residues include G57, G62, Y138, F300, L306, and E406.
e. Superposition of hBGT1–GABA (this study, light blue) and hNET bound to norepinephrine (PDB: 8ZPB, pale yellow). Key residues are labeled: N75, A145, Y152, F317, F323, and G423.

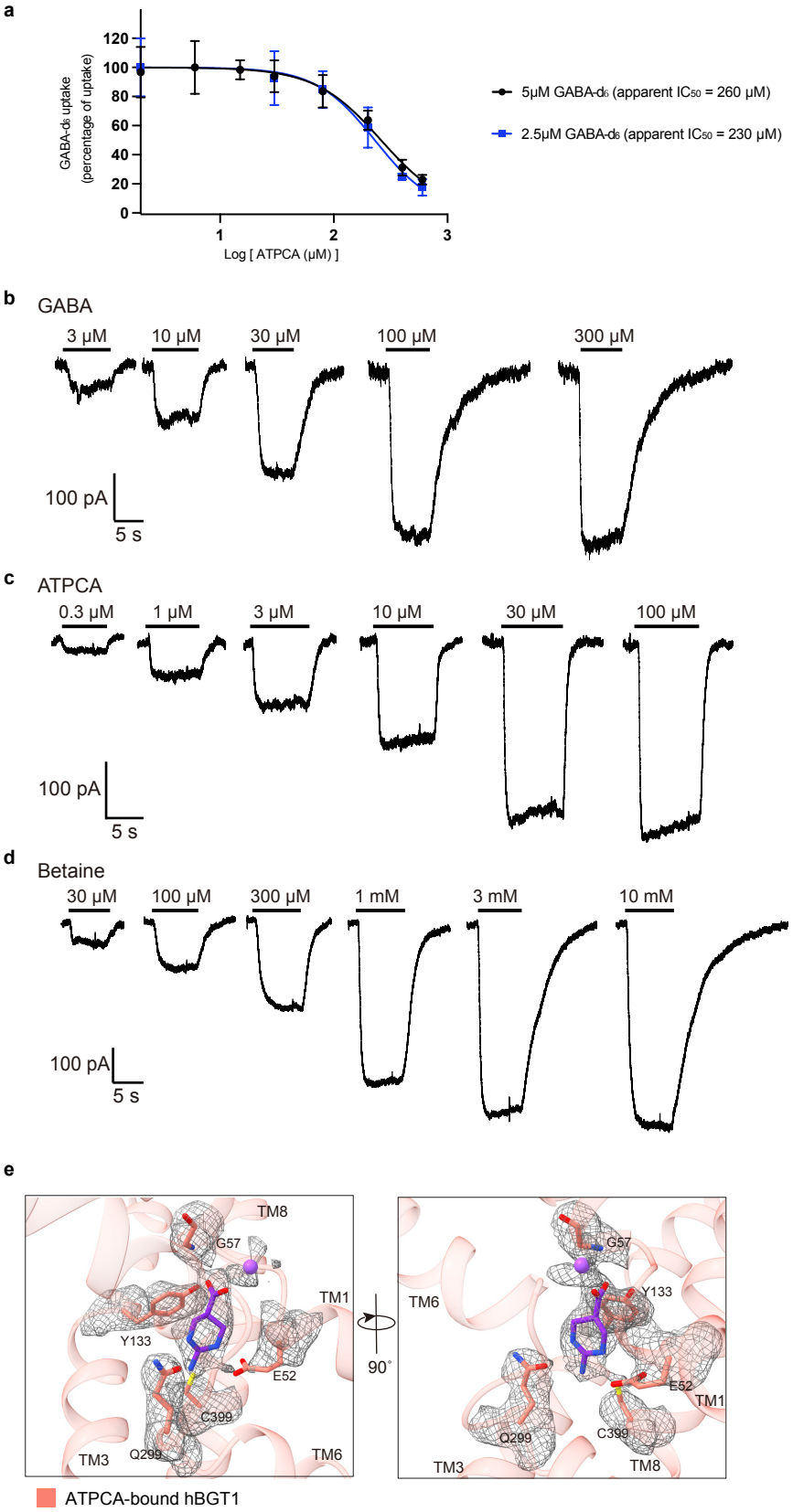

Supplementary Fig. 8 | ATPCA inhibition under LC–MS uptake conditions and representative electrophysiological traces of BGT1 substrates.
a. Dose–response curves showing the apparent half-maximal inhibitory concentration (IC_{50}) of ATPCA on GABA-d_6 uptake by hBGT1 under LC–MS–based uptake conditions at two GABA-d_6 concentrations (5 μM and 2.5 μM). Error bars represent the standard error of the mean (s.e.m.) from three independent experiments (n=3). Source data are provided as a Source Data file.
b–d. Representative traces of concentration-dependent inward currents elicited by GABA (b), ATPCA (c) and betaine (d) in BGT1-expressing HEK293T cells. Scale bars, 100 pA and 5 s.
e. Two orthogonal views of the substrate-binding pocket in ATPCA-bound hBGT1, with ATPCA and surrounding binding-site residues shown simultaneously in the cryo-EM density map (gray mesh), contoured at 5σ. Key interacting residues are labeled.

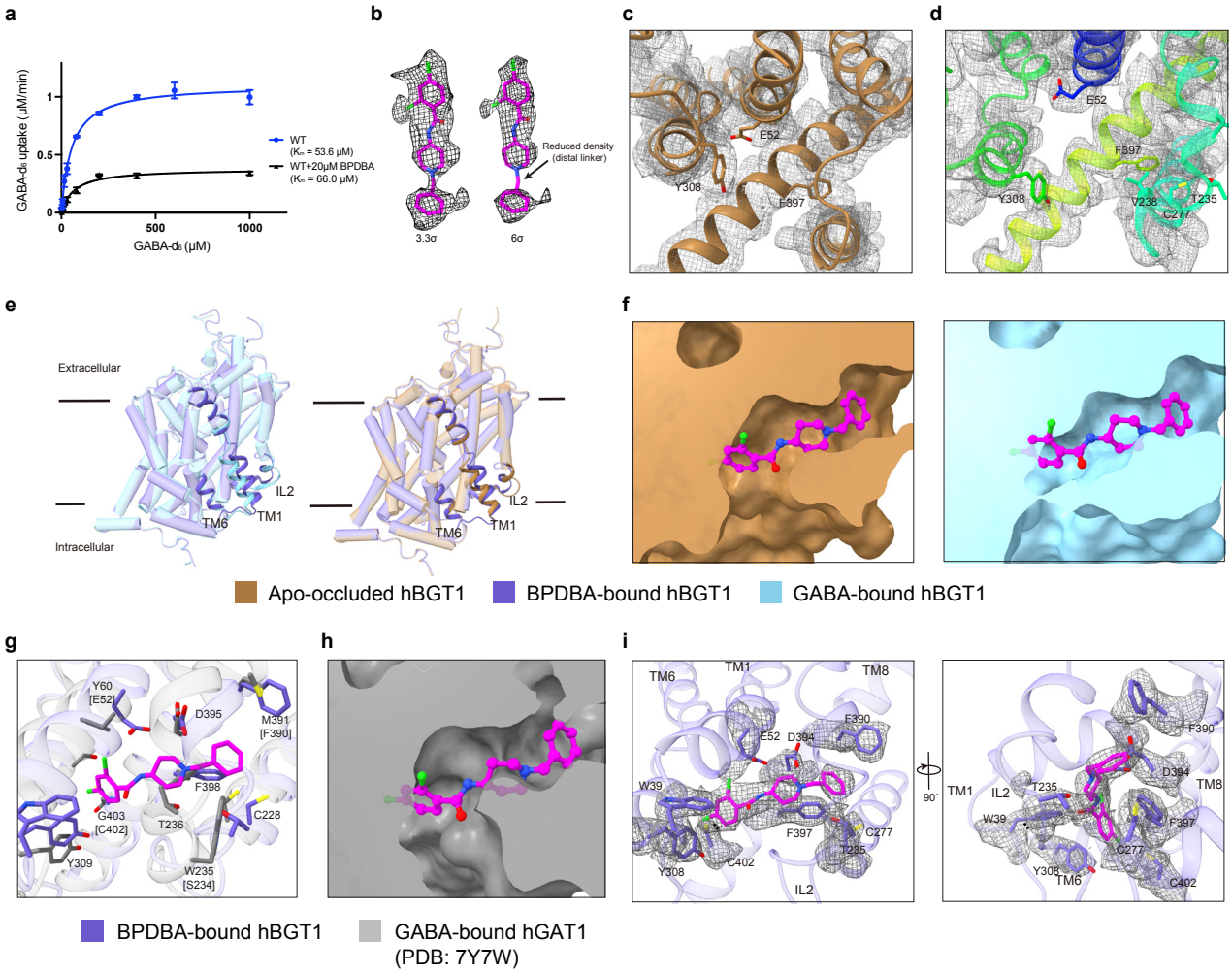

Supplementary Fig. 9 | Comparison of the BPDBA binding site.
a. Transport kinetics of wild-type hBGT1 in the absence or presence of 20 μM BPDBA. Transport was quantified by uptake assays using GABA-d_6 and fitted to the Michaelis–Menten equation. Wild-type hBGT1 is shown as blue circles with the corresponding fitted curve, and wild-type hBGT1 incubated with 20 μM BPDBA is shown as black triangles with the corresponding fitted curve. Error bars represent the standard error of the mean (s.e.m.) from three independent experiments (n = 3). Source data are provided as a Source Data file.
b. Cryo-EM density of BPDBA contoured at 3.3σ (left) and 6σ (right).
c. Cryo-EM density of the same region in the apo-occluded structure, contoured at 5.34σ. No ligand-like density is observed.
d. Cryo-EM density of the same region in the apo-inward structure, contoured at 5.34σ. No ligand-like density is observed.
e. Structural comparison of hBGT1 in the BPDBA-bound state and the occluded conformation. (Left) Superposition of BPDBA-bound (slate blue) and GABA-bound (light blue) structures. (Right) Superposition of BPDBA-bound (slate blue) and apo-occluded (brown) structures.
f. Surface representation of the BPDBA-binding pocket in the apo-occluded (left, brown) and GABA-bound (right, light blue) hBGT1 structures.
g. Structural alignment of hBGT1–BPDBA (this study, magenta) and hGAT1–GABA (PDB: 7Y7W, grey). The homologous region is enlarged (right) with key residues labeled: Y60, C228, W235, Y309, D395, M391, F398, and G403.
h. Clipped surface view of the homologous BPDBA-binding region in hGAT1, showing the spatial fit of BPDBA modeled from hBGT1
i. Two orthogonal views of the BPDBA-binding pocket in BPDBA-bound hBGT1, with BPDBA and surrounding pocket residues shown simultaneously in the cryo-EM density map (gray mesh), contoured at 5σ. Key interacting residues are labeled.

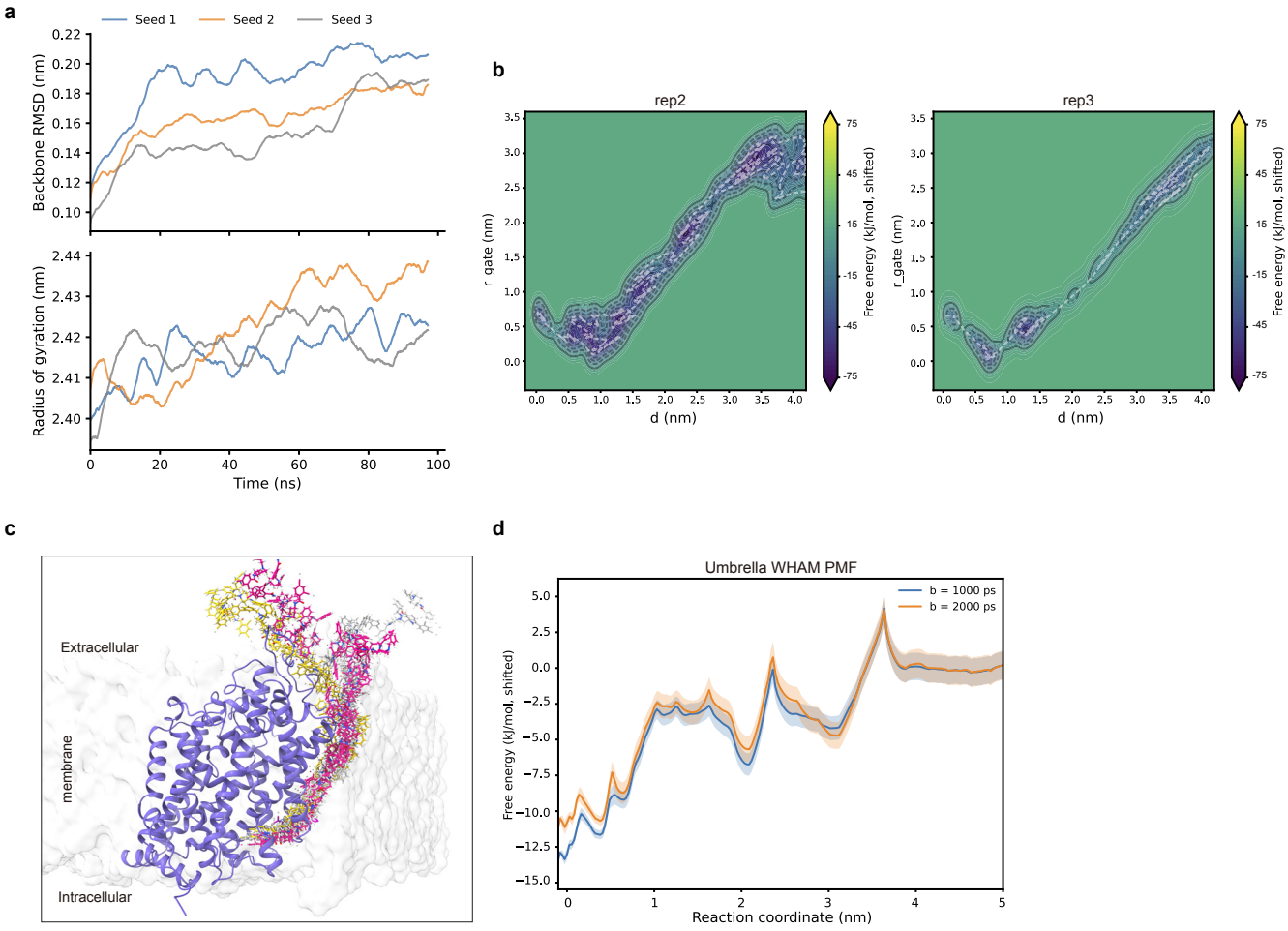

Supplementary Fig. 10 | Reproducibility and auxiliary analyses of MD simulations.
a. Protein backbone RMSD and radius of gyration (Rg) of hBGT1 monitored during three independent conventional MD simulations of the BPDBA-bound state. Rolling averages are shown to reduce high-frequency noise and facilitate comparison across trajectories.
b. Two-dimensional free-energy surfaces projected onto (d, r_gate) from metadynamics replicas 2 and 3, plotted using the same collective variable ranges and free-energy scale as in Fig. 5f. The dashed line indicates a representative metadynamics sampling trajectory projected onto the same collective variable space. The overall topology of the free-energy landscape and the dissociation corridor are preserved across independent simulations.
c. Reproducibility of SMD dissociation pathways across independent simulations. Overlay of BPDBA positional distributions obtained from three independent SMD simulations initiated from the cryo-EM–derived BPDBA-bound state. For each replica, ligand positions sampled along the driven dissociation trajectory are rendered as clouds after alignment of the protein backbone. The overlap of the spatial distributions highlights the consistency of the dissociation pathway sampled under external driving forces across independent simulations.
d. Umbrella sampling potential of mean force derived from the SMD dissociation trajectory. One-dimensional potential of mean force (PMF) reconstructed by umbrella sampling and WHAM analysis along the reaction coordinate defined by the SMD dissociation pathway (replica 1). The PMF was calculated using trajectory segments excluding the initial 1000ps or 2000 ps of each umbrella window (b = 1000 ps or b = 2000 ps). Solid lines show re-zeroed PMF profiles, and shaded regions represent bootstrap errors from the WHAM analysis (PMF ± bootstrap error).

Supplementary Table 1 | Cryo-EM data collection, refinement, and validation statistics

	The apo state hBGT1 in the inward-facing conformation	The apo state hBGT1 in the occluded conformation	The betaine-bound hBGT1	The GABA-bound hBGT1	The ATPCA-bound hBGT1	The BPDBA-bound hBGT1
PDB ID	9W9B	9W9C	9W99	9W9A	9W98	9W97
EMDB ID	EMD-65769	EMD-65770	EMD-65767	EMD-65768	EMD-65766	EMD-65765
Data collection and processing						
Magnification	81,000 ×	81,000 ×	64,000 ×	81,000 ×	81,000 ×	81,000 ×
Voltage (kV)	300	300	300	300	300	300
Electron exposure (e–/Å^2)	50	50	60	50	50	50
Defocus range (μm)	-1.5 to -1.8	-1.5 to -1.8	-1.5 to -1.8	-1.5 to -1.8	-1.5 to -1.8	-1.5 to -1.8
Pixel size (Å)	1.067	1.067	1.08	1.067	1.067	1.067
Symmetry imposed	C1	C1	C1	C1	C1	C1
Initial particle images (no.)	4,555,377	4,559,256	2,779,194	5,115,650	4,851,122	6,185,120
Final particle images (no.)	145,802	92,699	162,073	137,106	153,144	92,959
Map resolution (Å)	2.87	3.02	3.04	2.98	2.71	2.84
FSC threshold	0.143	0.143	0.143	0.143	0.143	0.143
Map resolution range (Å)	250-2.87	250-3.02	250-3.04	250-2.98	250-2.71	250-2.84
Map sharpening B factor (Å^2)	-117.7	-125.1	-122.3	-126.1	-114.2	-113.2
Refinement						
Initial model used	Alphafold3 model	Alphafold3 model	Alphafold3 model	Alphafold3 model	Alphafold3 model	Alphafold3 model
Model resolution (Å)	3.1	3.3	3.2	3.2	2.9	3.0
FSC threshold	0.5	0.5	0.5	0.5	0.5	0.5
Model resolution range (Å)	250-3.1	250-3.3	250-3.2	250-3.2	250-2.9	250-3.0
Model composition						
Non-hydrogen atoms	4315	4296	4369	4375	4330	4377
Protein residues	536	534	541	542	536	540
Ligands	1	0	4	4	4	2
B factors (Å^2)						
Protein	81.99	92.21	68.95	69.70	69.00	53.77
Ligand	87.85	--	61.43	34.29	31.19	21.22
R.m.s. deviations						
Bond lengths (Å)	0.002	0.003	0.002	0.004	0.004	0.003
Bond angles (°)	0.464	0.463	0.448	0.519	0.543	0.503
Validation						
MolProbity score	1.32	1.35	1.33	1.48	1.36	1.30
Clashscore	5.79	5.35	5.96	6.17	6.47	5.38
Poor rotamers (%)	0.00	0.00	0.00	0.00	0.00	0.00
CaBLAM outliers (%)	0.76	0.57	0.56	0.75	0.57	0.75
Ramachandran plot						
Favored (%)	99.06	97.74	98.14	97.21	98.31	97.95
Allowed (%)	0.94	2.26	1.86	2.79	1.69	2.05
Disallowed	0.00	0.00	0.00	0.00	0.00	0.00
Model content	hBGT1: 40-172, 181-583 Ligand: Cl^-	hBGT1: 41-172, 182-583	hBGT1: 35-172, 182-584 Ligand: Na^+, Cl^-, betaine	hBGT1: 36-171, 179-584 Ligand: Na^+, Cl^-, GABA	hBGT1: 39-172, 182-583 Ligand: Na^+, Cl^-, ATPCA	hBGT1: 36-172, 181-583 Ligand: Cl^-, BPDBA

The parameters for the Cryo-EM data collection, processing, and validation for the structures of hBGT1 in the apo, the betaine-bound, the GABA-bound, the ATPCA-bound and the BPDBA-bound states are listed in the table.

Supplementary Table 2 | Summary of molecular dynamics simulation systems

Parameter	Free BPDBA system	BPDBA-bound hBGT1 system
Protein	hBGT1 (apo-inward conformation)	hBGT1 (BPDBA-bound state)
Initial coordinates	Cryo-EM–derived apo-inward hBGT1 structure	Cryo-EM–derived BPDBA-bound hBGT1 structure
Ligands	25 BPDBA molecules placed in extracellular solvent	One BPDBA molecule bound in the intracellular pocket
Force field	CHARMM36m	CHARMM36m
Water model	TIP3P	TIP3P
Lipid composition	Outer leaflet: POPC/SSM/CHL1 = 35/25/40 (mol%) Inner leaflet: POPC/POPE/POPS/POPI/CHL1 = 10/35/25/15/15 (mol%)	Same as free BPDBA system
System construction	CHARMM-GUI membrane builder	CHARMM-GUI membrane builder
Ion concentration	150 mM NaCl	150 mM NaCl
Simulation box	Rectangular box with periodic boundary conditions	Rectangular box with periodic boundary conditions
Approximate box dimensions	11.4 × 11.4 × 13.3 nm^3	9.9 × 9.9 × 12.2 nm^3
Total number of water molecules	40941	26356
Total number of atoms	176647	122459
Temperature	310K	310K
Pressure	1 bar (semi-isotropic coupling)	1 bar (semi-isotropic coupling)
MD engine	GROMACS 2025.4	GROMACS 2025.4
Enhanced sampling	None (unbiased MD)	Well-tempered metadynamics and steered MD (where indicated)
Number of replicas	3	3

Supplementary Table 3 | Primer sequences used for construct generation and mutagenesis

Construct / mutant	Forward primer sequence (5'–3')	Reverse primer sequence (5'–3')
hBGT1	CAAGGCCCTGAATTCATGGACGGGAAGGTGGCAGTG	GTGGTGGTGCTCGAGTCACAAATGGGTCTCCTTCTC
E52Y	GCCGGGTACATCATTGGGCTGGGCAAT	AATGATGTACCCGGCCACTGACAG
E52A	GCCGGGGCCATCATTGGGCTGGGCAAT	AATGATGGCCCCGGCCACTGACAG
Q299A	ATCTGCGCAGGGTGCCTGACAGCC	GCACCCTGCGCAGATGGCAAAGGAGAAGAA
G57A	GGGCTGGCGAATGTCTGGAGGTTTCCCTAT	GACATTCGCCAGCCCAATGATCTCCCC
Y133A	GTCTACGCAATCATCATCCTTGCCTGG	GATGATTGCGTAGACATTCAAATATGACTCGATGAC
C402A	GTGGAGGCACTGGTGACAGCCTCCATAGAC	CACCAGTGCCTCCACACAGACAAACTGGCT
C402S	GTGGAGTCACTGGTGACAGCCTCCATAGAC	CACCAGTGACTCCACACAGACAAACTG

Supplementary Fig. 11a | Uncropped SDS–PAGE corresponding to Supplementary Fig. 1a
Full-length SDS–PAGE gel showing size-exclusion chromatography fractions of purified hBGT1.
Lane M: molecular weight marker
Lanes 13.0–17.5 mL: SEC fractions collected as indicated above the gel
Fractions 14.0–15.5 mL (highlighted in Supplementary Fig. 1a) were pooled for subsequent structural studies and are presented in Supplementary Fig. 1a (inset).
No lanes were removed or rearranged.

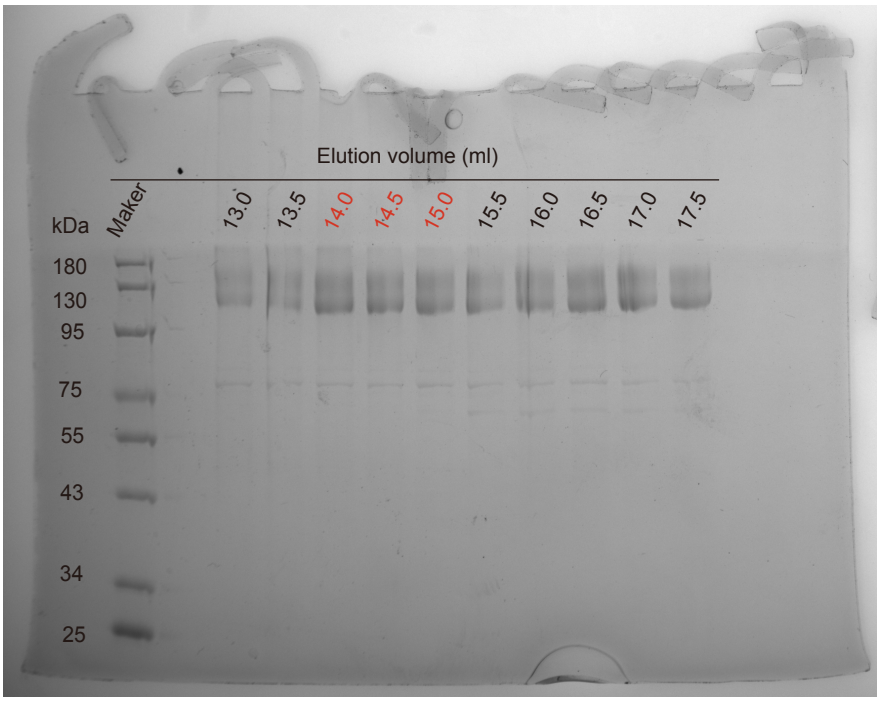

Supplementary Fig. 11b | Uncropped immunoblot corresponding to Supplementary Fig. 1c
Full-length western blot showing expression of GFP–MBP-tagged and non-tagged hBGT1 constructs in HEK293T cells.
Lane 1: GFP–MBP-tagged hBGT1
Lane 2: Non-tagged hBGT1
Lanes 3-6: Additional constructs analyzed in the same experiment (not shown in Supplementary Fig. 1c).
Lanes 1–2 were used in Supplementary Fig. 1c.
No lanes were removed or rearranged.